IJMMM International Journal of Minerals, Metallurgy and Materials 矿物冶金与材料学报（英文版）

Flotation separation of scheelite from calcite using luteolin as a novel depressant

Xiaokang Li, Ying Zhang, Haiyang He, Yu Wu, Danyu Wu, and Zhenhao Guan

Cite this article as:
Xiaokang Li, Ying Zhang, Haiyang He, Yu Wu, Danyu Wu, and Zhenhao Guan, Flotation separation of scheelite from calcite using luteolin as a novel depressant, *Int. J. Miner. Metall. Mater.*, 31(2024), No. 3, pp. 462-472. https://doi.org/10.1007/s12613-023-2755-x

---

Articles you may be interested in

IJMMM WeChat

QQ author group

INTERNATIONAL JOURNAL OF
Minerals, Metallurgy and Materials

Volume 31, Number 3, March 2024
Page 462

Research Article https://doi.org/10.1007/s12613-023-2755-x

Flotation separation of scheelite from calcite using luteolin as a novel depressant

Xiaokang Li[1)], *Ying Zhang*[1,2),✉], *Haiyang He*[1)], *Yu Wu*[1)], *Danyu Wu*[1)], *and Zhenhao Guan*[1)]

1) Faculty of Land and Resources Engineering, Kunming University of Science and Technology, Kunming 650093, China
2) State Key Laboratory of Clean Utilization of Complex Non-Ferrous Metal Resources, Kunming University of Science and Technology, Kunming 650093, China
(Received: 4 July 2023; revised: 25 September 2023; accepted: 26 September 2023)

Abstract: This paper proposes luteolin (LUT) as a novel depressant for the flotation-based separation of scheelite and calcite in a sodium oleate (NaOL) system. The suitability of LUT as a calcite depressant is confirmed through micro-flotation testing. At pH = 9, with LUT concentration of 50 mg·L^{-1} and NaOL concentration of 50 mg·L^{-1}, scheelite recovery reaches 80.3%. Calcite, on the other hand, exhibits a recovery rate of 17.6%, indicating a significant difference in floatability between the two minerals. Subsequently, the surface modifications of scheelite and calcite following LUT treatment are characterized using adsorption capacity testing, Zeta potential analysis, Fourier transform infrared spectroscopy (FT-IR), X-ray photoelectron spectroscopy (XPS), and atomic force microscopy (AFM). The study investigates the selective depressant mechanism of LUT on calcite. Adsorption capacity testing and Zeta potential analysis demonstrate substantial absorption of LUT on the surface of calcite, impeding the further adsorption of sodium oleate, while its impact on scheelite is minimal. FT-IR and XPS analyses reveal the selective adsorption of LUT onto the surface of calcite, forming strong chemisorption bonds between the hydroxyl group and calcium ions present. AFM directly illustrates the distinct adsorption densities of LUT on the two mineral types. Consequently, LUT can effectively serve as a depressant for calcite, enabling the successful separation of scheelite and calcite.

Keywords: scheelite; calcite; luteolin; flotation; depressant; separation

1. Introduction

Tungsten is an important metal in national strategic reserves due to its properties such as high density, melting point, hardness, and wear resistance and it is widely applied in various industries, including mining and metallurgy, aerospace, military, machinery, construction, electronics, and chemicals, earning the nickname of "industrial teeth" [1]. Historically, tungsten resources have primarily been developed and utilized from wolframite. However, with economic growth, the demand for tungsten resources has increased, resulting in the depletion of easily accessible wolframite deposits. Therefore, it is urgent need to explore and exploit scheelite resources [2]. Flotation is a major method employed to recover scheelite ($CaWO_4$), calcite ($CaCO_3$) is a representative gangue mineral associated with scheelite, it is not easy to do the flotation separation of the two minerals. Firstly, the surfaces of scheelite and calcite are subjected to interconversion in the pulp, therefore the selectivity of the agent to the mineral surface is reduced. Secondly, the ions dissolved on the surface of calcium bearing minerals affect the pulp environment by changing the pH of the scheelite pulp and reacting with the reagents, influencing the expected flotation of scheelite flotation. Finally, mineral surfaces are difficult to separate because they have similar flotation behavior and identical active particles and crystal structures. Therefore, the separation of scheelite and calcite has remained a challenging task in the efficient recovery of scheelite resources [3].

Sodium oleate (NaOL) is a commonly used fatty acid collector in scheelite flotation. However, due to the poor selectivity, additional selective depressants are typically required to inhibit calcium-containing gangue minerals [4]. Depressants for scheelite can be categorized as inorganic or organic. Inorganic depressants, such as water glass, are commonly used but are pH-dependent and have a limited flotation range [5]. On the other hand, organic depressants like tannin, pectin, starch, carboxymethyl cellulose (CMC), and sodium polyacrylate (PA-Na) offer advantages such as easy customization, wide availability, and variety [6–7]. However, part of organic depressant synthesis routes leads to greater environmental pollution, poor stability, and high price [8–9]. Given these shortcomings of traditional depressants, it is necessary to develop new high-performance flotation depressants.

Luteolin (LUT), also known as 3',4',5,7-tetrahydroxyflavone, is a natural flavonoid found in various plants. It appears as a pale-yellow powder and has a structural formula (Fig. 1) with a chemical formula of $C_{15}H_{10}O_6$ and a molecular weight of 286.23. Currently, luteolin is primarily used in clinical medicine as an antitussive, expectorant, and anti-inflammatory drug [10]. Its molecular chain contains multiple

✉ Corresponding author: Ying Zhang E-mail: zhyingcsu@163.com

hydroxyl groups, making it highly hydrophilic and capable of chelating with metallic elements on mineral surfaces. However, it has not yet been applied in mineral separation, and its interaction mechanism with various minerals remains unknown. This paper introduces LUT as a novel depressant for the flotation separation of scheelite and calcite. Furthermore, the study investigates the mechanism of LUT's interaction with mineral surfaces.

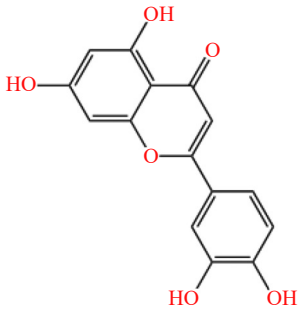

Fig. 1. Chemical structure of luteolin.

2. Experimental

2.1. Minerals and reagents

Scheelite and calcite minerals were obtained from the Xuebaoding mining area in Wuping County, Sichuan Province and Shilin County, Yunnan Province, respectively. The mineral samples were manually sorted to eliminate gangue minerals. A portion of the samples was polished for contact angle measurement, while the remaining portions were crushed, ground using a three-head grinder, and screened with various screen sizes according to test standards. Slice samples were utilized for contact angle measurement, and particles ranging in size from 38 to 75 μm were used for micro-flotation tests, including X-ray diffraction (XRD), atomic force microscopy (AFM), Fourier transform infrared spectroscopy (FT-IR), and X-ray photoelectron spectroscopy (XPS). Samples with a particle size below 38 μm were further ground in an agate bowl, and the resulting samples below 2 μm were utilized for Zeta potential testing. XRD analysis of the samples reveals only the characteristic peaks of scheelite and calcite, indicating high mineral purity (Fig. 2). The mineral composition analysis is presented in Table 1, which demonstrates a calcite purity of 97.7% and a scheelite purity of 92.94%, meeting the testing requirements. Deionized water with an electrical resistivity of 18.25 MΩ is used throughout the experiments, and the analysis results of deionized water are shown in Table 2. In the flotation tests, LUT was employed as a depressant, NaOL served as the collector, and HCl and NaOH were used to adjust the required pH. All flotation reagents were analytical pure grade.

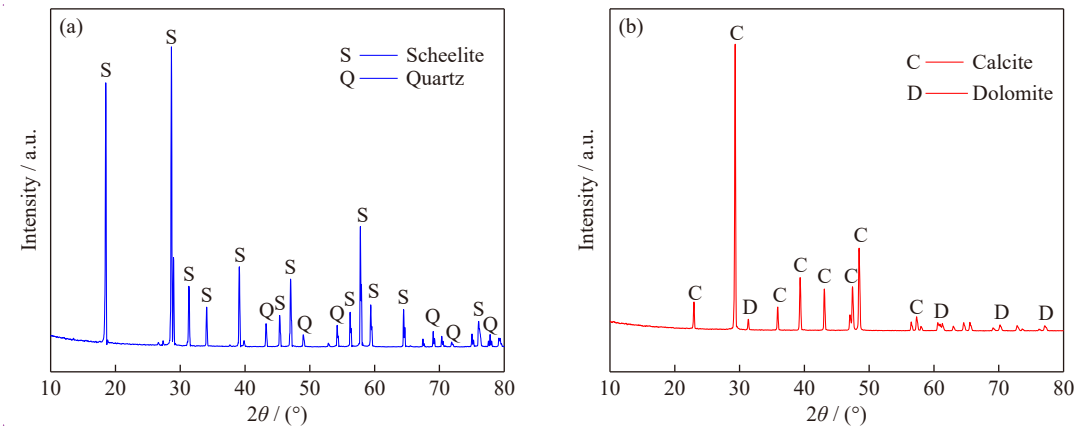

Fig. 2. XRD pattern of (a) scheelite and (b) calcite.

2.2. Micro-flotation test

The micro-flotation tests were conducted using a 40 mL FGC hanging cell flotation machine (Wuhan Luoke Co., Ltd.). In each test, approximately 2 g of a single pure mineral was weighed and added to the flotation tank along with deionized water, maintaining a pulp volume of 40 mL. The stirring speed was set at 1600 r·min^{-1}. The test procedure is depicted in Fig. 3. Initially, the pulp was stirred for 1 min, followed by pH adjustment to the desired test conditions within 2 min. Subsequently, the depressant LUT and the collector NaOL were sequentially added. The interaction time and flotation time for each reagent with the minerals were set at 3 min. The recovery of a single mineral flotation was calculated using Eq. (1). The mixed minerals are composed of scheelite and calcite by mass ratio of 1:1, and the WO_3 grade of the mixed minerals is 33.4wt%. The recovery of the mixed minerals was calculated by recording the yield and measuring the WO_3 grades of the product using Eq. (2):

$$\varepsilon_1 = \frac{m_1}{m_1 + m_2} \times 100\% \quad (1)$$

where m_1 is the weight of the concentrate, m_2 is the weight of the tailings, and ε_1 is the recovery rate.

$$\varepsilon_2 = \gamma \frac{\beta - \theta}{\alpha - \theta} \times 100\% \quad (2)$$

where ε_2 represents the recovery rate of WO_3, γ represents the yield of the concentrate, and β, θ, and α represent the grade of WO_3 in the concentrate, tailing, and raw mineral, respectively.

Table 1. Main components in mineral samples wt%

Minerals	WO_3	CaO	MgO	SiO_2
Scheelite	79.85	13.09	—	0.28
Calcite	—	54.70	0.30	—

Table 2. Analysis results of deionized water

Ions	Concentration / ($mg \cdot L^{-1}$)
Ca	<0.10
Na	10.6
Mg	<0.01
Zn	<0.02
Al	<0.01
Fe	<0.01

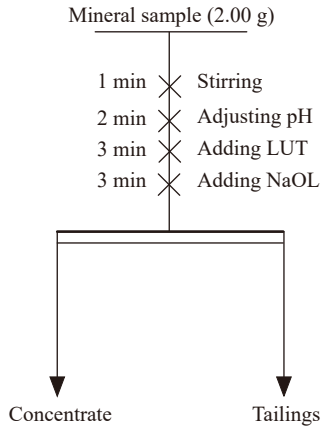

Fig. 3. Micro-flotation flowsheet of pure minerals.

2.3. Adsorption capacity test

2.3.1. Drawing of standard curves

The UV-2700 UV-visible spectrophotometer was employed as the testing instrument. The following steps were conducted for the tests: standard solutions of luteolin with varying concentration gradients were prepared, with deionized water serving as the reference solution for full spectrum scanning. The results revealed that the absorption peak was most pronounced at a wavelength of 326.4 nm. Hence, the absorbance values of the reagents at different concentration were determined at $\lambda = 326.4$ nm, as illustrated in Fig. 4. The relationship between the reagents and absorbance aligned with the Bouguer-Lambert-Beer Law [11].

2.3.2. Adsorption measurement

The experimental procedure involved filtering the pulp following the reagent treatment. The supernatant obtained after centrifugation was utilized as the sample for adsorption testing, with photometric determination conducted. The concentration of the reagent in the solution was measured, and calculations were performed according to the following formula.

$$\tau = (C_0 - C)V/(mA) \quad (3)$$

where τ represents the adsorption density of the reagent on the mineral surface ($mg \cdot m^{-2}$), C_0 is the reagent concentration in the pulp before treatment ($mg \cdot L^{-1}$), C is the reagent concentration in the pulp after treatment ($mg \cdot L^{-1}$), V represents the volume of the solution (L), m is the weight of the sample (g), and A is the specific surface area of the mineral powder ($m^2 \cdot g^{-1}$), as outlined in Table 3.

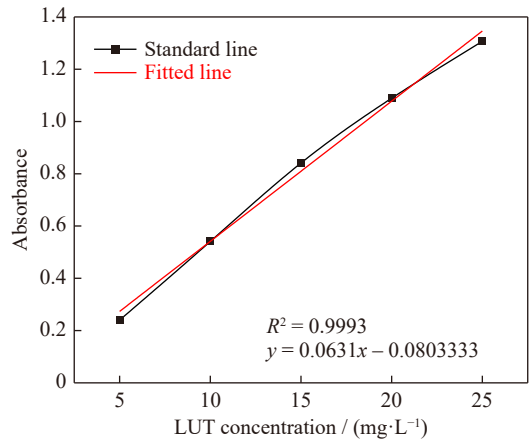

Fig. 4. Relationship between LUT concentration and absorbance ($\lambda = 326.4$ nm).

Table 3. Specific surface area of pure minerals

Minerals	Specific surface area / ($m^2 \cdot g^{-1}$)
Scheelite	0.2533
Calcite	0.2597

2.4. Zeta potential test

Zeta potential measurements were conducted using the Zetasizer Nano Zs90 potentiometer (Malvern, UK). To prepare the samples, the pure minerals were ground in an agate mortar until achieving a particle size below 2 μm. Then, 20 mg of the samples were weighed and placed in a beaker. Subsequently, 40 mL of a potassium chloride electrolyte solution with a concentration of 5×10^{-3} $mol \cdot L^{-1}$ was added, and the mixture was stirred using a magnetic stirrer at a rotation speed of 800 $r \cdot min^{-1}$ for 2 min. The reagent was then added according to the flotation test's reagent system. After stirring for 15 min, the reagent was removed, and the beaker was allowed to stand for 5 min. A suitable amount of the upper suspension was collected using a straw and transferred to the electrophoresis cell for potential measurement. Each sample was measured three times under identical conditions, and the average value was considered as the test result.

2.5. Fourier transform infrared spectroscopy (FT-IR)

The FT-IR spectra were examined using the Bruker Alpha infrared spectrometer (Germany). The procedure involved stirring a single mineral in a beaker and adding a measured quantity of the reagent, following the same process as in the flotation experiment. Each reagent was stirred for a duration of 25 min. After mixing, the mixture was filtered using filter paper, rinsed with deionized water, and naturally air-dried before sampling for infrared testing. The scanning range was set between 400 and 4000 cm^{-1}, with 16 scanning repetitions and a spectral resolution of 4 cm^{-1}.

2.6. X-ray photoelectron spectroscopy (XPS)

XPS test is employed to analyze the chemical composi-

tion and chemical state of elements on the mineral surface. In the sample preparation process, the pH of the entire pulp system was initially adjusted, followed by the addition of the reagent according to the flotation process's reagent system. The mixture was stirred using a magnetic stirrer at a rotation speed of 750 r·min^{-1}, then filtered using filter paper, rinsed three times with deionized water of the same pH value, and air-dried naturally. For this study, the PHI5000 Versaprobe-II device with an aluminum target emitting Kα rays as the X-ray source was utilized. Each test was conducted with a voltage maintained at 15 kV, power set to 50 W, full-spectrum passing energy at 46.95 eV, and a step size of 0.2 eV. The test data were fitted using Multipak software (version 9.3.0.3), and all binding energies were calibrated with the C 1s carbon peak at 284.8 eV.

2.7. Atomic force microscope (AFM)

AFM is a surface characterization technique that enables the imaging of pharmaceutical agent adsorption on mineral surfaces. The two-dimensional geometry and three-dimensional height morphology of the hemimorphic ore under different conditions were acquired using an atomic force microscope. The Bruker Dimension Icon instrument was employed, with a mineral scanning range of 5 μm × 5 μm. Prior to each test, the sample holder was meticulously cleaned using acetone and ethanol, rinsed with ample deionized water to eliminate any residual contaminants, and gently dried using ultra-high purity nitrogen. The probe was cleaned in a UV chamber for approximately 30 min. A mica substrate used for measuring sample particles was cleaned using tape. The sample was affixed to a glass plate for detection. The SCANASYST-AIR cantilever model was utilized, and the scanning rate was set to 0.8 Hz. Finally, the obtained images were processed using Nano Scope Analysis software.

3. Results and discussion

3.1. Micro-flotation test

Fig. 5(a) illustrates the effect of NaOL concentration on the flotation recovery of scheelite and calcite. When only NaOL was added, the recovery of scheelite and calcite increased as the NaOL concentration increased. At the NaOL concentration of 50 mg·L^{-1}, the recovery rate was 84.7% and 89.9% for scheelite and calcite, respectively, indicating similar floatability. However, once the NaOL concentration surpassed 50 mg·L^{-1}, the recovery of reached a balance. The result demonstrated that without the addition of a depressant, NaOL alone was insufficient to achieve effective separation through flotation.

Fig. 5(b) demonstrates the impact of introducing the depressant LUT on the flotation recovery rates of scheelite and calcite at different pH levels of the pulp. In the absence of LUT, both scheelite and calcite exhibit an increase in recovery rates with rising pH values, and a slight decrease when pH above 9. Within the tested range (pH = 6–11), the flotation behavior of the two minerals is similar when LUT is not

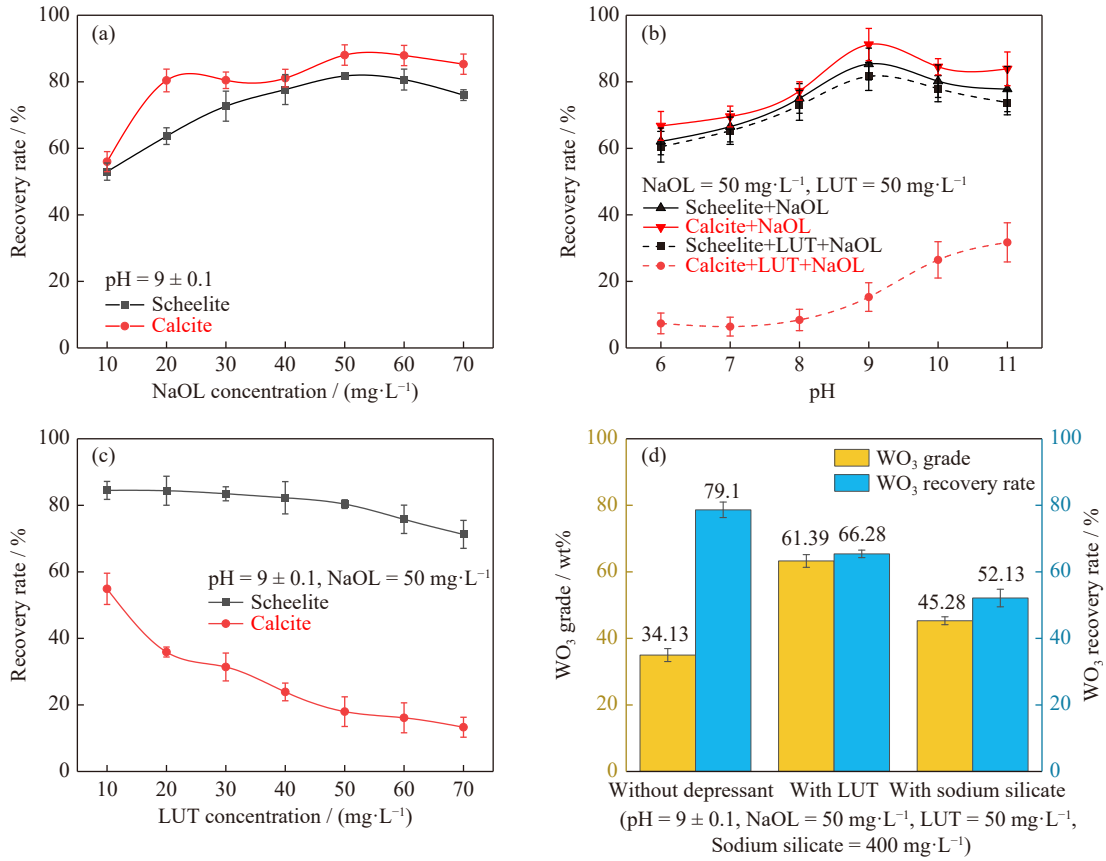

Fig. 5. Effect of (a) NaOL concentration, (b) pH, and (c) LUT concentration on the flotation recovery of scheelite and calcite; (d) sorting efficiency.

added. At pH 9, the recovery rates of scheelite and calcite reach 85.4% and 91.5%, respectively. These results indicate that altering the pH of the pulp alone presents challenges in effectively separating the two minerals. Upon the addition of LUT, a slight decrease in scheelite recovery rate is observed. The relationship between recovery rate and pH becomes more pronounced as pH increases, reaching a maximum at pH 9. Subsequently, the recovery rate exhibits a gradual decline as pH continues to rise. On the other hand, the recovery of calcite experiences a sharp decrease upon the addition of LUT, with the depressant effect of LUT weakening as pH increases. At pH levels below 9, the recovery rate of calcite remains below 15%. These findings demonstrate that the addition of LUT enhances the disparity in floatability between the two minerals. Notably, at pH 9, the largest discrepancy in recovery rates is observed, with scheelite reaching 81.8% and calcite only 15.54%, resulting in a significant difference of 66.27%. Thus, the condition of pH 9 is selected for further tests.

Fig. 5(c) illustrates the depressant effect of LUT concentration on the two minerals. LUT demonstrates minimal depressive effect on scheelite, with the recovery rate of scheelite decreasing only slightly as LUT concentration increases. When the LUT concentration is below 50 mg·L^{-1}, the recovery rate of scheelite remains above 80%. However, excessive LUT concentration also leads to a noticeable decrease in scheelite recovery rate. On the other hand, the results indicate that LUT effectively depresses calcite. As the LUT concentration increases, the recovery rate of calcite decreases significantly. When the LUT concentration exceeds 50 mg·L^{-1}, the recovery rate of calcite stabilizes at approximately 15%. At the LUT concentration of 50 mg·L^{-1}, the recovery rate of scheelite is 80.3%, while that of calcite is 17.6%. These findings highlight the selective depressant effect of LUT on calcite, increasing the disparity in floatability between the two minerals. This creates favorable conditions for flotation separation and indicates the potential of LUT as a depressant in the flotation separation of scheelite and calcite.

Fig. 5(d) presents the impact of LUT on the sorting efficiency of mixed ore, with NaOL concentration of 50 mg·L^{-1} and a pH value of 9. Without the addition of LUT, the concentrate exhibits the WO_3 grade of 34.13wt%, and the recovery rate of 79.1%. This indicates that it is challenging to effectively separate scheelite and calcite using NaOL alone in the absence of inhibitors. However, with a LUT concentration of 50 mg·L^{-1}, the WO_3 grade significantly improves to 61.39wt% and the recovery rate is 66.28%. To investigate the inhibitory performance of LUT, it is compared with traditional inhibitor sodium silicate. The results demonstrate that LUT achieves a favorable sorting effect at low dosage, offering cleaner and more efficient separation. Moreover, LUT is non-toxic, harmless, and minimally pollute to the environment. Therefore, the findings from the mixed mineral flotation test affirm that LUT is an environmentally friendly and cost-effective selective inhibitor for the flotation separation of scheelite and calcite.

3.2. Adsorption capacity test

The selective adsorption of LUT on the mineral surfaces of scheelite and calcite can be directly observed through measurements and calculations of the adsorption density. Fig. 6 demonstrates notable differences in the adsorption density of LUT on the surfaces of the two minerals. Specifically, the adsorption density of LUT on scheelite surfaces is relatively low, exhibiting a gradual increase with rising LUT concentration. The adsorption density ranges from 0.35 to 1.65 mg·m^{-2}. In contrast, the adsorption density on calcite surfaces ranges from 1.03 to 5.42 mg·m^{-2}. With an increase in LUT concentration, the adsorption density significantly rises, surpassing that of scheelite. At a LUT concentration of 50 mg·L^{-1}, the adsorption density on the surface of scheelite is merely 1.65 mg·m^{-2}, while on the surface of calcite, it reaches 5.42 mg·m^{-2}. These results corroborate the selective adsorption of LUT on the surface of calcite, aligning with the findings of the micro-flotation tests.

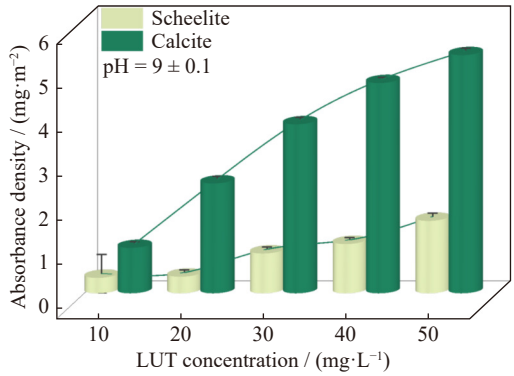

Fig. 6. Adsorption density of LUT on scheelite and calcite as a function of LUT concentration.

3.3. Zeta potential test

Fig. 7 depict the impact of pH conditions on the Zeta potential of scheelite and calcite under various reagent conditions. In Fig. 7(a), no isoelectric point of scheelite is observed within the tested pH range (pH = 6–11). The Zeta potential of scheelite raw ore exhibits a negative trend as the pH value increases. This negativity is attributed to the presence of negatively charged WO_4^{2-} ions on the surface of scheelite, consistent with previous result [12]. Upon the addition of LUT, the Zeta potential of scheelite experiences a slight negative shift. This can be attributed to the abundance of negatively charged hydroxyl groups in LUT, which can interact with the surface of scheelite. As a result, at pH 9, the Zeta potential of scheelite raw ore is –21.7 mV, and after adding LUT, the Zeta potential becomes –28.9 mV, exhibiting a negative shift of 7.2 mV. Furthermore, when NaOL is subsequently added, a significant additional shift in potential is observed. This is likely due to the reaction of NaOL with the scheelite surface in the form of oleic acid groups, which carry a negative charge. Consequently, the Zeta potential of scheelite experiences a further negative shift [13]. Specifically, at pH 9, after the sequential addition of LUT and NaOL, the

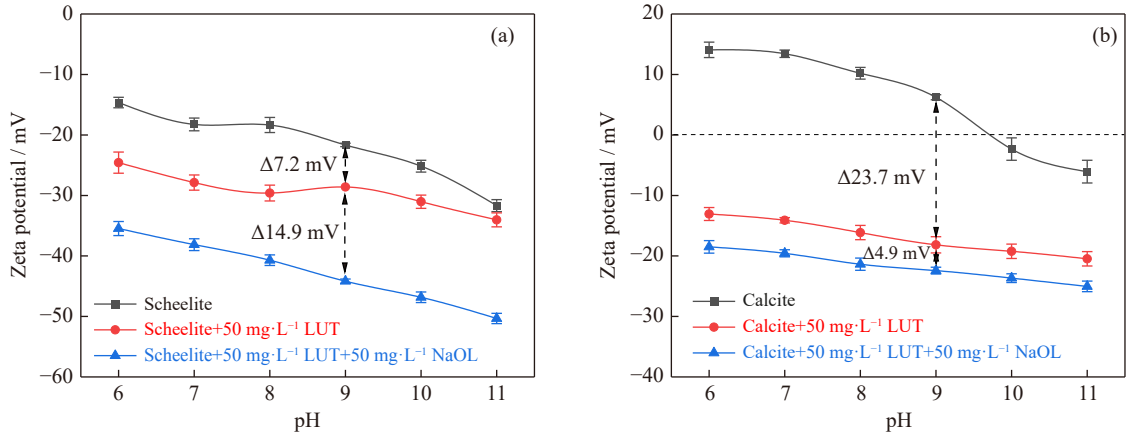

Fig. 7. Zeta potential of (a) scheelite and (b) calcite as a function of pH.

Zeta potential of scheelite is –43.8 mV, reflecting a negative shift of 14.9 mV compared to the addition of LUT alone. These results demonstrate that NaOL can still effectively react with the scheelite surface following the action of LUT.

Fig. 7(b) illustrates the pH corresponding to isoelectric point of calcite is approximately 9.5. Below pH = 9.5, the potential of calcite is positive due to the presence of positively charged Ca^{2+} ions on its surface [14]. The Zeta potential of calcite decreases as pH increases. However, upon the addition of LUT, a significant negative shift in the Zeta potential of calcite is observed. At pH = 9, the potential of raw calcite ore is 6.1 mV. After reacting with LUT, the potential of calcite becomes –17.6 mV, indicating a substantial negative shift of 23.7 mV. This shift is notably higher than that of scheelite, and it is speculated that the abundant negatively charged hydroxyl groups in LUT react with calcium ions on the surface of calcite, resulting in a negative potential shift. Interestingly, the potential of calcite is –22.5 mV after adding NaOL, representing a minor negative shift of only 4.9 mV. This suggests that the reaction of a significant amount of LUT with calcite impedes the further adsorption of sodium oleate. Through the analysis of the Zeta potential, it can be concluded that LUT visibly reacts with calcite and hinders the subsequent adsorption of sodium oleate, while its influence on scheelite is limited.

3.4. FT-IR analysis

Fig. 8 displays the FT-IR spectra of NaOL and LUT. In Fig. 8(a), the characteristic peaks at 2921.74 and 2851.51 cm^{-1} correspond to the stretching vibrations of methyl and methylene groups in NaOL molecules. The peaks observed at 1560.18 and 1446.28 cm^{-1} are attributed to the asymmetric and symmetric vibration peaks of carboxyl groups [15]. Notably, there are distinct characteristic peaks at 3413.47 cm^{-1}, which may be associated with the vibrations of bound water molecules [16]. In Fig. 8(b), the spectral band at 3400.14 cm^{-1} corresponds to the peaks generated by the stretching vibrations of –OH groups and the stretching of intermolecular and intramolecular hydrogen bonds. The peaks at 1615.64 and 1515.06 cm^{-1} represent the skeleton vibrations of the benzene ring. Additionally, the peak at 1657.53 cm^{-1} is the characteristic peak of the carbonyl group [17].

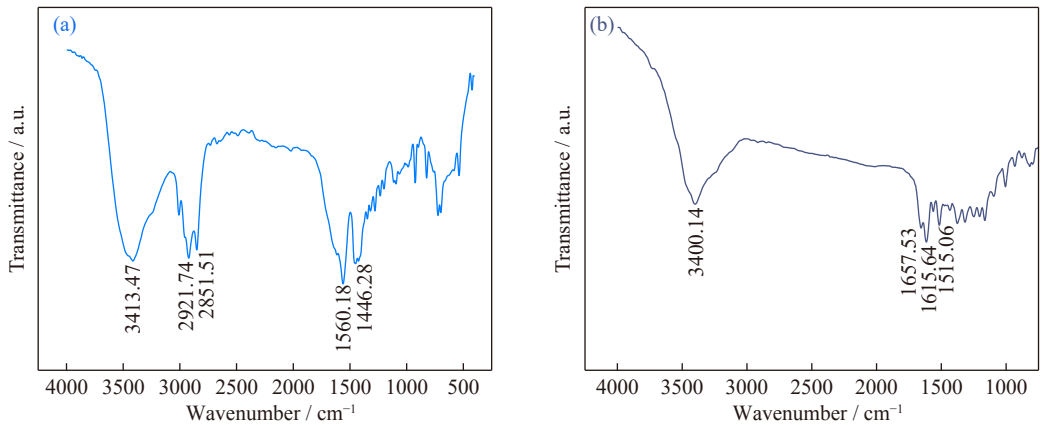

Fig. 8. FT-IR spectra of (a) NaOL and (b) LUT.

Fig. 9(a) illustrates the variations in the infrared spectrum of scheelite before and after the interaction with different agents. In the spectrum of raw scheelite ore, characteristic peaks at 814 and 440 cm^{-1} arise from the stretching and bending vibrations of W–O bonds [12]. Upon reacting with LUT, the spectrum of scheelite shows no significant changes, and no new characteristic peaks emerge. However, after treating scheelite with LUT followed by NaOL, new characteristic peaks appear at 2923 and 2850 cm^{-1}, corresponding to the characteristic peaks of methyl and methylene groups in NaOL. Based on the infrared spectrum analysis before and after the addition of scheelite, it can be concluded that the interac-

tion between LUT and scheelite is relatively weak. Moreover, the reaction between LUT and scheelite does not impede the subsequent reaction with NaOL, which aligns with the findings obtained from the Zeta potential analysis.

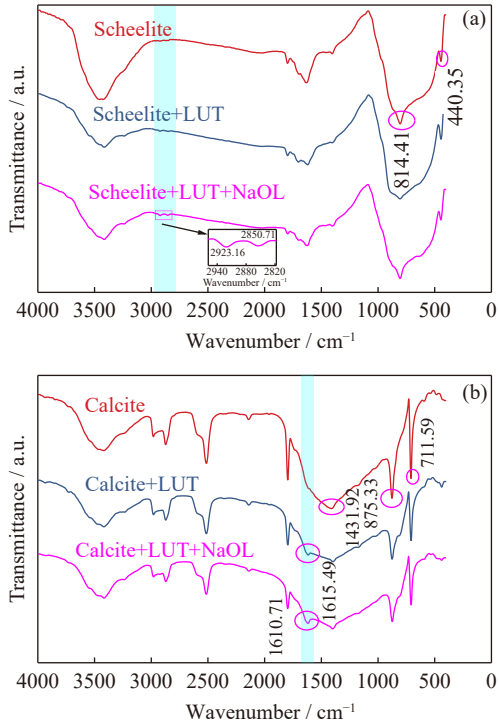

Fig. 9. FT-IR spectra of (a) scheelite and (b) calcite before and after the reaction of reagents.

Fig. 9(b) depicts the alterations in the infrared spectrum of calcite under the influence of different agents. In the spectrum of raw calcite ore, the characteristic peaks at 1431.92 cm^{-1} corresponded to the stretching vibration of C–O bonds, while the deformation vibration of C–O results in the characteristic peaks at 857.33 and 711.59 cm^{-1} [18]. Following the interaction of calcite with LUT, in addition to the aforementioned characteristic peaks, a newly formed peak was observed at 1615.49 cm^{-1} in the spectrum. This peak was attributed to the 1610.71 cm^{-1} characteristic peak of the benzene ring in LUT, which shifted 4.78 cm^{-1} to the right. This shift suggested that LUT chemisorbs onto the surface of calcite. After treating calcite with LUT and NaOL, only the characteristic peaks of LUT mentioned earlier were evident in the spectrum, and no characteristic peaks attributed to NaOL were observed. This indicated that LUT effectively hindered the reaction between NaOL and calcite, preventing their interaction.

3.5. XPS analysis

Fig. 10(a) presents the high-resolution XPS spectra of C 1s before and after the addition of LUT to calcite. As can be seen, two well-fitted peaks of C 1s are observed in raw calcite at 289.4 and 284.8 eV. The peak at 289.4 eV corresponds to carbon presented in calcite, while the peak at 284.8 eV is associated with carbon–oxygen compounds [19]. Following the interaction of calcite with LUT, a prominent fitted peak emerges at 286.3 eV. This peak is attributed to C–OH in LUT molecules, indicating a change in the chemical environment of carbon on the surface of calcite before and after the action of LUT [20]. These findings suggest that LUT chemisorbs onto the calcite surface.

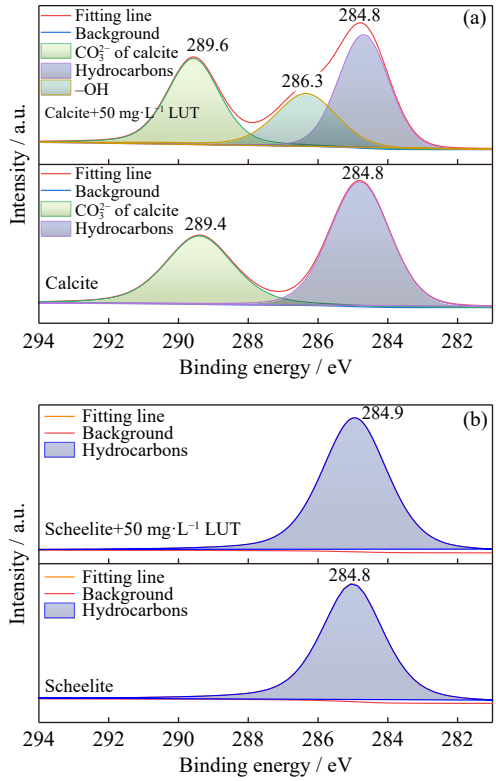

Fig. 10. Fitting peaks of C 1s on the (a) calcite and (b) scheelite surface before and after adding LUT.

The molecular formula of scheelite ($CaWO_4$) does not contain carbon. However, during sample preparation in an open environment, it can be susceptible to carbon contamination from the air. In Fig. 10(b), a distinct peak at 284.8 eV was observed in the C 1s high-resolution XPS spectrum of raw scheelite ore, which could be attributed to carbon oxides formed on the surface of scheelite due to air pollution. Upon reaction with LUT, no significant changes were observed in the C 1s spectrum of scheelite, and no new peaks emerged [21]. The peak at 284.8 eV in the raw ore underwent a slight shift to 284.9 eV, with a deviation of 0.1 eV, which falls within the test error range (instrument error used by the testing institution ≤0.4 eV). This indicated that the chemical environment of carbon on the surface of scheelite remained unchanged after the action of LUT, and LUT does not adsorb onto the scheelite surface.

The changes in the O 1s spectrum of calcite before and after interaction with LUT are depicted in Fig. 11(a). A distinct peak at 531.6 eV was observed in the raw calcite ore, attributed to oxygen in the carbonates of calcite [22]. After the interaction between calcite and LUT, in addition to the original peak, a fitted peak emerged at 533.1 eV, corresponding to C–OH in the LUT molecule [23].

In Fig. 11(b), scheelite exhibited a separation peak at 530.6 eV, resulting from oxygen in the WO_4^{2-} of scheelite it-

self [24]. No significant changes were observed in the spectrum of scheelite after its interaction with LUT. The analysis indicated that LUT could selectively adsorb onto the surface of calcite, forming chelation with calcium ions on the calcite surface through the C–OH group in the LUT molecule, thereby firmly adsorbing to the calcite surface.

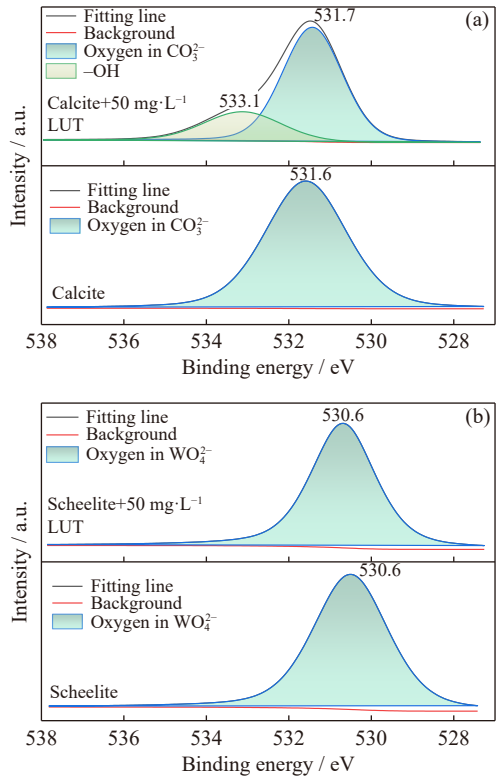

Fig. 11. Fitting peaks of O 1s on the (a) calcite and (b) scheelite surface before and after adding LUT.

Table 4 presents the relative concentrations of calcium, carbon, and oxygen on the surface of scheelite and calcite after the reaction with LUT. To ensure comparability between the two minerals, the relative concentrations only consider calcium, carbon, and oxygen (excluding tungsten) in scheelite. Upon reacting with LUT, the relative carbon content on the surface of scheelite increased by 0.99wt%, while the relative calcium and oxygen elements decreased by 0.49wt% each. In the case of combined LUT and calcite interaction, the relative carbon content increased by 1.86wt%, surpassing the increase observed on the surface of scheelite (0.99wt%). On the other hand, the relative calcium and oxygen concent decreased by 1.04wt% and 0.82wt%, respectively. The increase in carbon concentration signified the substantial carbon content present in LUT molecules, which adsorb onto the surface of calcite, resulting in an elevated carbon concentration. The decrease in calcium and oxygen concentrations could be attributed to the adsorption of depressants covering these elements on the mineral surface and the corresponding decrease due to the increased carbon content. This demonstrates the significant adsorption capacity of LUT on the surface of calcite, indicating a stronger depressant effect of LUT on calcite compared to scheelite, aligning with previous research findings.

Table 4. Atomic concentration on the surface of scheelite and calcite

Samples	Atomic concentration / mol%		
	C 1s	O 1s	Ca 2p
Scheelite	30.48	58.39	11.13
Scheelite+LUT	31.46	57.90	10.64
Δ_1	0.98	–0.49	–0.49
Calcite	41.14	46.85	12.00
Calcite+LUT	43.00	45.81	11.18
Δ_2	1.86	–1.04	–0.82

Notes: Δ_1 and Δ_2 represent the difference between scheelite and scheelite+LUT and calcite and calcite+LUT, respectively.

3.6. AFM analysis

AFM analysis allows for the direct visualization of the adsorption morphology of LUT on the mineral surface following the interaction of scheelite and calcite. Figs. 12–13 depict the two-dimensional (2D) geometric topography and three-dimensional (3D) height topography, respectively, before and after the interaction of scheelite, calcite, and LUT. Table 5 presents the R_q and R_a values, which represent the RMS (Root mean square) deviation and arithmetic mean of absolute height deviation, respectively, allowing for the comparison of changes in mineral surface roughness pre- and post-agent interaction.

Fig. 12(a) illustrates the surface of untreated scheelite ore exhibits low roughness (R_q = 2.26 nm and R_a = 1.75 nm) and relatively smooth, thereby excluding the influence of mineral morphology on agent adsorption. On the other hand, Fig. 12(b) depicts the surface topography characteristics following the interaction between scheelite and LUT. A slight increase in surface roughness was observed (R_q = 3.40 nm and R_a = 2.48 nm) compared to the original scheelite surface. Referring to the vertical axis, the 3D scanning image revealed the presence of small white bumps, overall presenting a darker brown color, indicating the surface of scheelite is relatively flat and minimal LUT adsorption on the scheelite surface.

Fig. 13 presents the surface roughness of untreated calcite ore is R_a = 5.75 nm and R_q = 4.68 nm. Compared to the scheelite surface, the calcite surface exhibits greater roughness. The 2D image reveals spot-like distribution of calcite, while the 3D image showed the presence of outgrowths. Following the addition of LUT, there was a significant increase in surface roughness, with R_a = 10.31 nm and R_q = 8.68 nm, indicating a rougher calcite surface. The 2D image displays a dense block distribution of LUT on the calcite surface, and the height of protrusions in the 3D image is noticeably amplified. Referring to the vertical axis, there is a significant color change in the 3D image of calcite: from the original predominantly brown color to a large number of white protrusions. The color difference indicates that the selective adsorption of LUT on the calcite surface, with a considerably higher adsorption density compared to scheelite, aligning with the results obtained from previous experiments.

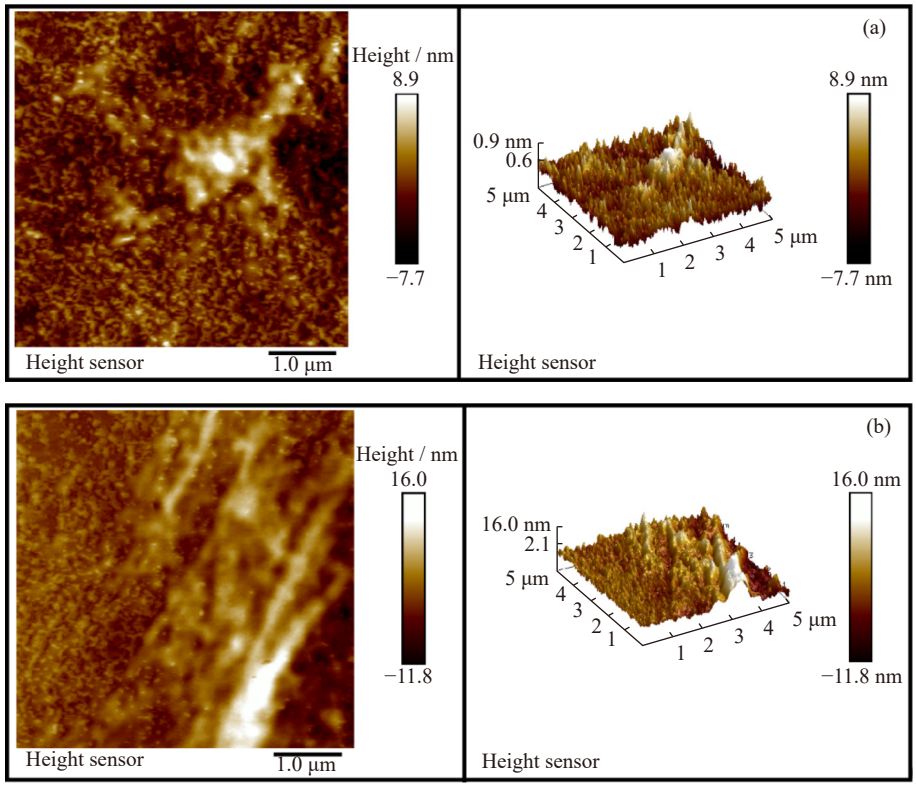

Fig. 12. AFM images of (a) scheelite and (b) scheelite+LUT (left: height; right: 3D).

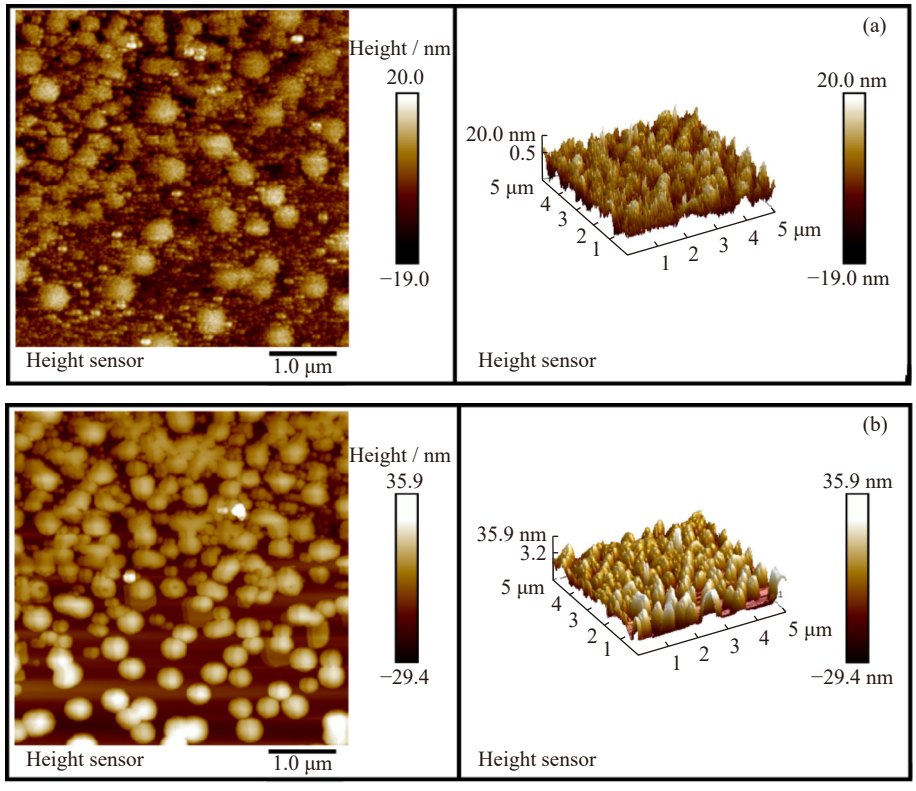

Fig. 13. AFM images of (a) calcite and (b) calcite+LUT (left: height; right: 3D).

3.7. Adsorption model of the agents

LUT is primarily extracted from peanut shells and other agricultural crops. Traditionally, peanut shells have been regarded as waste or either disposed of or incinerated in agricultural practices. However, these methods not only contribute to atmospheric contaminate but also poses safety risks. Remarkably, peanut shells contain about 0.3wt% of luteolin, which represents a rich and inexpensive resources. The application of LUT as an inhibitor in the flotation separation of calcite scheelite requires a relatively small amount. This not only reduces the cost of the agent but also promotes the pro-

Table 5. Surface roughness of scheelite and calcite

Minerals	R_q / nm	R_a / nm
Scheelite	2.26	1.75
Scheelite+LUT	3.40	2.48
Calcite	5.75	4.68
Calcite+LUT	10.31	8.68

tection of ecological environment by facilitating the utilization of solid waste. Consequently, this utilization of LUT from peanut shells holds significant economic potential and practical importance. Based on the aforementioned series of mechanistic studies, this work developed a separation model for scheelite and calcite in the NaOL system, employing LUT as a depressant (Fig. 14). The disparity in adsorption density and strength of LUT on the mineral surfaces can be attributed to the different surface properties of the two minerals [25]. The scheelite surface is predominantly occupied by negatively charged WO_4^{2-}, this charge distribution leads to electrostatic repulsion between the hydroxyl groups in LUT molecules and the scheelite surface, limiting the availability of calcium sites for LUT adsorption. Conversely, the calcite surface is predominantly occupied by positively charged Ca^{2+}, offering ample calcium sites for firm chelation of the hydroxyl groups in LUT molecules through chemisorption. This selective adsorption significantly impedes the subsequent adsorption of sodium oleate on the calcite surface. The impact on scheelite, however, is minimal, increasing the difference in floatability between the two minerals and enabling their effective separation.

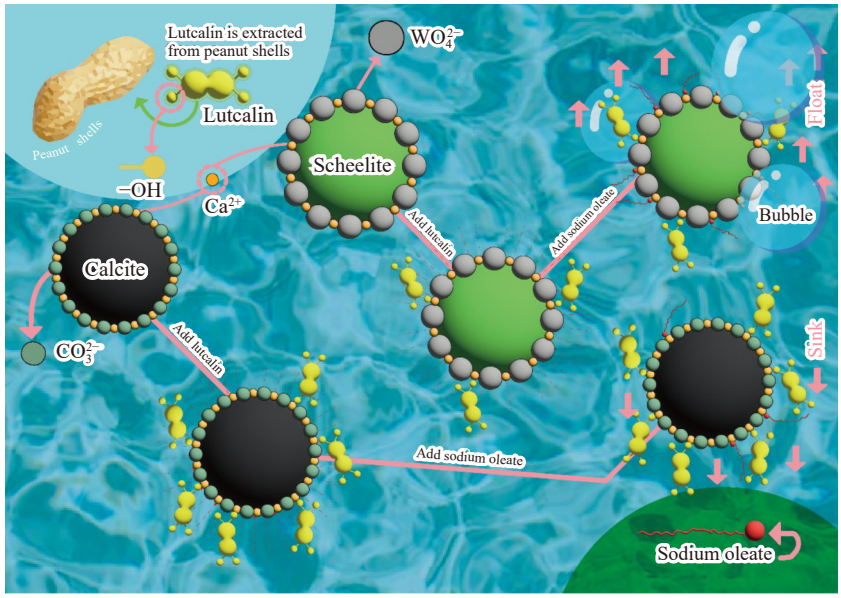

Fig. 14. Schematic of the flotation separation of scheelite and calcite.

4. Conclusions

This study reports that LUT serves as an effective depressant for the flotation separation of scheelite and calcite, yielding the following key findings:

(1) Single mineral tests reveal that at pH = 9, the recovery rate of scheelite with a sodium oleate concentration of 50 mg·L^{-1} reaches 80.3%, whereas that of calcite is only 17.6%. LUT selectively inhibits calcite while having minimal impact on scheelite.

(2) Adsorption capacity and Zeta potential tests demonstrate that LUT exhibits selective adsorption on calcite, with a significantly higher adsorption amount compared to scheelite. The extensive adsorption of LUT on the surface of calcite hampers the subsequent adsorption of sodium oleate, whereas its influence on scheelite is negligible.

(3) FT-IR and XPS analyses confirm that the addition of LUT to calcite results in the appearance of characteristic peaks in the infrared spectrum attributed to LUT, while the spectrum of scheelite remains unchanged. Subsequent addition of NaOL does not alter the spectrum of calcite, whereas the infrared spectrum of scheelite exhibits characteristic peaks of NaOL. XPS analysis reveals that LUT predominantly interacts with the surface of calcite through C–OH components and undergoes chemisorption, a process that is more pronounced than in the case of scheelite.

(4) AFM imaging vividly illustrates the differential adsorption of LUT on the mineral surfaces. The surface roughness of calcite significantly increases after LUT treatment compared to scheelite, indicating the strong selective adsorption of LUT on calcite. This disparity in adsorption leads to the distinct floatability of scheelite and calcite, facilitating their effective separation.

Acknowledgements

This study was financially supported by the National Natural Science Foundation of China (No. 52164022).

Conflict of Interest

All authors declare no competing financial interest.

References

[1] A. Talignani, R. Seede, A. Whitt, *et al*., A review on additive manufacturing of refractory tungsten and tungsten alloys, *Addit. Manuf.*, 58(2022), art. No. 103009.

[2] X. Wang, W.Q. Qin, F. Jiao, *et al*., Review of tungsten resource reserves, tungsten concentrate production and tungsten beneficiation technology in China, *Trans. Nonferrous Met. Soc. China*, 32(2022), No. 7, p. 2318.

[3] Z.M. Wang, B. Feng, and Y.G. Chen, Flotation separation depressants for scheelite and calcium-bearing minerals: A review, *Int. J. Miner. Metall. Mater.*, 30(2023), No. 9, p. 1621.

[4] J.J. Wang, Z.Y. Gao, H.S. Han, W. Sun, Y.S. Gao, and S. Ren, Impact of NaOL as an accelerator on the selective separation of scheelite from fluorite using a novel self-assembled Pb–BHA–NaOL collector system, *Appl. Surf. Sci.*, 537(2021), art. No. 147778.

[5] S.Y. Zhang, J.Z. Kuang, M.M. Yu, W.Q. Yuan, and Z.Y. Huang, Effect of ultrasonication of sodium silicate on selective adsorption of scheelite and fluorite surfaces, *Colloids Surf. A*, 642(2022), art. No. 128633.

[6] Y. Foucaud, I.V. Filippova, and L.O. Filippov, Investigation of the depressants involved in the selective flotation of scheelite from apatite, fluorite, and calcium silicates: Focus on the sodium silicate/sodium carbonate system, *Powder Technol.*, 352(2019), p. 501.

[7] F. Jiao, L.Y. Dong, W.Q. Qin, W. Liu, and C.Q. Hu, Flotation separation of scheelite from calcite using pectin as depressant, *Miner. Eng.*, 136(2019), p. 120.

[8] R.L. Wang, W.J. Sun, H.S. Han, W. Sun, Z. Wei, and J. Peng, Al-caustic starch coordination compounds: A new depressant for fine calcite, *Colloids Surf. A*, 648(2022), art. No. 129268.

[9] Z.M. Wang, B. Feng, and Y.G. Chen, The separation behavior and mechanism of scheelite and dolomite using locust bean gum as depressant, *Miner. Eng.*, 202(2023), art. No. 108280.

[10] P. Prasher, M. Sharma, S.K. Singh, *et al*., Luteolin: A flavonoid with a multifaceted anticancer potential, *Cancer Cell Int.*, 22(2022), No. 1, art. No. 386.

[11] C. Marrassini, A. Idrissi, I. De Waele, *et al*., Organic solvent–luteolin interactions studied by FT-Raman, Vis-Raman, UV-Raman spectroscopy and DFT calculations, *J. Mol. Liq.*, 205(2015), p. 2.

[12] M.A.M. Abdalla, H.Q. Peng, H.A. Younus, D. Wu, L. Abusin, and H. Shao, Effect of synthesized mustard soap on the scheelite surface during flotation, *Colloids Surf. A*, 548(2018), p. 108.

[13] H.L. Han, W.Z. Yin, B. Yang, D.H. Wang, J. Yao, and Z.L. Zhu, Adsorption behavior of sodium oleate on iron minerals and its effect on flotation kinetics, *Colloids Surf. A*, 647(2022), art. No. 129108.

[14] D. Yang, B.Q. Li, D.X. Feng, *et al*., Flotation separation of smithsonite from calcite with guar gum as depressant, *Colloids Surf. A*, 650(2022), art. No. 129562.

[15] J.W. Lu, Z.T. Yuan, M.M. Li, *et al*., The role of sodium oleate (NaOL) in the magnetic separation of pentlandite from serpentine using magnetic coating, *Powder Technol.*, 345(2019), p. 492.

[16] S.J. Bai, J. Li, Y.X. Bi, J.Q. Yuan, S.M. Wen, and Z. Ding, Adsorption of sodium oleate at the microfine hematite/aqueous solution interface and its consequences for flotation, *Int. J. Min. Sci. Technol.*, 33(2023), No. 1, p. 105.

[17] C. Chen, W. Zhao, W. Liu, *et al*., Research of dyeing thermodynamics and supramolecular structure of luteolin on wool fabric, *World J. Eng. Technol.*, 5(2017), No. 1, p. 19.

[18] D. Azizi and F. Larachi, Surface interactions and flotation behavior of calcite, dolomite and ankerite with alkyl hydroxamic acid bearing collector and sodium silicate, *Colloids Surf. A*, 537(2018), p. 126.

[19] L.Y. Dong, F. Jiao, W.Q. Qin, and W. Liu, Selective flotation of scheelite from calcite using xanthan gum as depressant, *Miner. Eng.*, 138(2019), p. 14.

[20] J. Liu, D.C. Kong, R.Q. Xie, Y.J. Li, Y.M. Zhu, and C. Liu, Flotation behavior and mechanism of hydroxycitric acid as a depressant on the flotation separation of cassiterite from calcite, *Miner. Eng.*, 170(2021), art. No. 107046.

[21] C.H. Zhong, H.H. Wang, B. Feng, L.Z. Zhang, Y.G. Chen, and Z.Y. Gao, Flotation separation of scheelite and apatite by polysaccharide depressant xanthan gum, *Miner. Eng.*, 170(2021), art. No. 107045.

[22] L.Y. Dong, L.D. Qiao, Q.F. Zheng, *et al*., Enhanced adsorption of citric acid at the calcite surface by adding copper ions: Flotation separation of scheelite from calcite, *Colloids Surf. A*, 663(2023), art. No. 131036.

[23] Q. Wei, L.Y. Dong, F. Jiao, and W.Q. Qin, Selective flotation separation of fluorite from calcite by using sesbania gum as depressant, *Miner. Eng.*, 174(2021), art. No. 107239.

[24] L.Y. Dong, Q. Wei, W.Q. Qin, and F. Jiao, Effect of iron ions as assistant depressant of citric acid on the flotation separation of scheelite from calcite, *Chem. Eng. Sci.*, 241(2021), art. No. 116720.

[25] L.Y. Dong, F. Jiao, W.Q. Qin, H.L. Zhu, and W.H. Jia, New insights into the carboxymethyl cellulose adsorption on scheelite and calcite: Adsorption mechanism, AFM imaging and adsorption model, *Appl. Surf. Sci.*, 463(2019), p. 105.